

Part 3. Sound Field Separation (SFS)

Yet Another Form of the Spherical Wave Function

A small confession is in order. Equations 2.1 was not used in the simulations computations in Part 2. The form below was used instead:

$$\hat{p}(r, \theta, \phi; \omega) = \sum_{n=0}^N \sum_{m=-n}^n [C_{mn} h_n^{(1)}(kr) + D_{mn} j_n(kr)] Y_n^m(\theta, \phi) \quad (3.1)$$

Not really a big deal since the various forms of the spherical wave expansion function can be readily transformed into each other. Recall:

$$\begin{aligned} h_n^{(1)}(kr) &= j_n(kr) + i y_n(kr) \\ \text{and} \quad h_n^{(2)}(kr) &= j_n(kr) - i y_n(kr) \end{aligned}$$

If we expand $C_{mn} h_n^{(1)}(kr) + D_{mn} j_n(kr)$:

$$\begin{aligned} C_{mn} h_n^{(1)}(kr) + D_{mn} j_n(kr) &= C_{mn} [j_n(kr) + i y_n(kr)] + D_{mn} j_n(kr) \\ &= [C_{mn} + D_{mn}] j_n(kr) + i C_{mn} y_n(kr) \end{aligned} \quad (3.2)$$

If we expand $A_{mn} h_n^{(1)}(kr) + B_{mn} h_n^{(2)}(kr)$ (see equation 2.1):

$$\begin{aligned} A_{mn} h_n^{(1)}(kr) + B_{mn} h_n^{(2)}(kr) &= A_{mn} [j_n(kr) + i y_n(kr)] + B_{mn} [j_n(kr) - i y_n(kr)] \\ &= [A_{mn} + B_{mn}] j_n(kr) + i [A_{mn} - B_{mn}] y_n(kr) \end{aligned} \quad (3.3)$$

Matching terms in equations 3.2 and 3.3:

$$\begin{aligned} C_{mn} &= A_{mn} - B_{mn} \\ \text{and} \quad D_{mn} &= 2B_{mn} \end{aligned} \quad (3.4)$$

With equations 3.4, we can interchange equations 3.1 and 2.1.

Sound Field Separation in Spherical Coordinates

In our non-anechoic measurements, we want to take our sound pressures measurements inside a *source free* measurement zone. The inner limit of this source free measurement zone is the spherical surface tangent to the outermost extremity of the interior sources and which center is the origin of our spherical coordinate system. The outer limit is a concentric spherical surface tangent to innermost extremity of the exterior sources. In practice, the inner and outer spherical surfaces do not need to be separated by too far a distance. The separation in the simulations was 0.1 m.

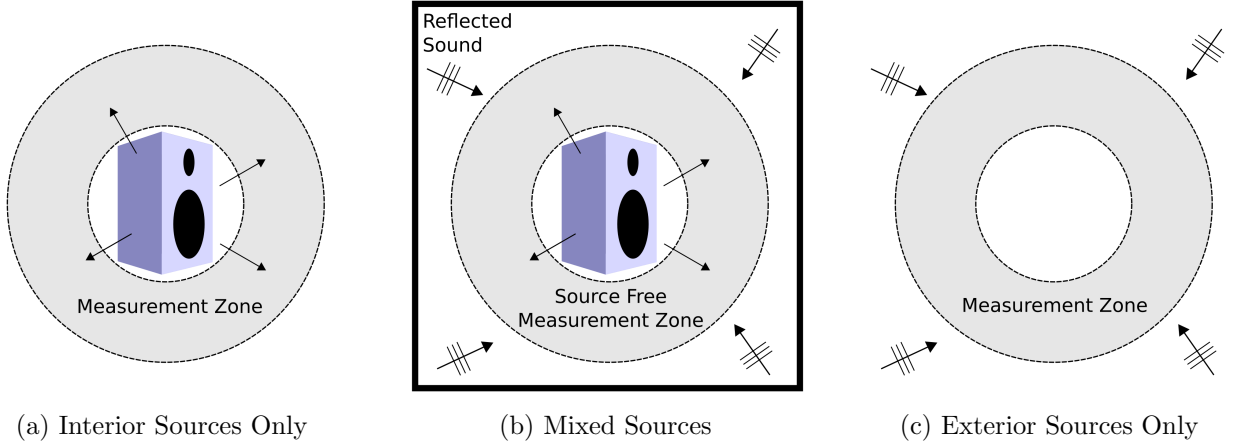


Figure 1: Sound Field Separation in Spherical Coordinates

When the sound source is completely within the inner limit of measurement zone as shown in Figure 1(a), there are only outgoing waves passing through the measurement zone. As the spherical Hankel functions of the first kind $h_n^{(1)}(kr)$ describes the outgoing waves, and the spherical Hankel functions of the second kind $h_n^{(2)}(kr)$ describes the incoming waves, the weighting coefficients for $h_n^{(2)}(kr)$ are zero. The spherical wave expansion functions for the interior sources only cases can be simplified to [1, p.21]:

$$\hat{p}(r, \theta, \phi; \omega)_{interior \ sources} = \sum_{n=0}^N \sum_{m=-n}^n C_{mn} h_n^{(1)}(kr) Y_n^m(\theta, \phi) \quad (3.5)$$

When the sound source is completely outside of the outer limit of measurement zone as shown in Figure 1(c), there are only standing waves in the measurement zone and we describe the spherical wave expansion functions using equation 1.1. As the spherical Bessel functions of the second kind $y_n(kr)$ is unbounded at $r = 0$ (they go to $-\infty$), the weighting coefficients for $y_n(kr)$ must all be zero. The spherical wave expansion functions for the exterior sources only cases can be simplified to [1, p.23]:

$$\hat{p}(r, \theta, \phi; \omega)_{exterior \ sources} = \sum_{n=0}^N \sum_{m=-n}^n D_{mn} j_n(kr) Y_n^m(\theta, \phi) \quad (3.6)$$

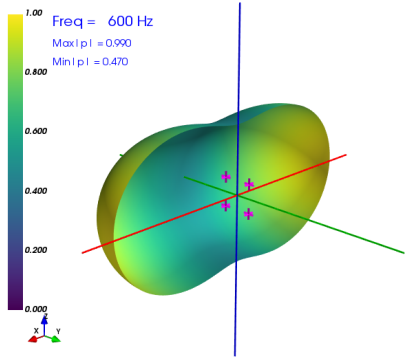
Since the Helmholtz equation is linear, when we have both exterior and interior sources, as in figure 1(b), the spherical wave expansion functions are the summation (superposition) of equations 3.5 and 3.6, which is equation 3.1 and is repeated below:

$$\hat{p}(r, \theta, \phi; \omega)_{mixed\ sources} = \sum_{n=0}^N \sum_{m=-n}^n [C_{mn}h_n^{(1)}(kr) + D_{mn}j_n(kr)] Y_n^m(\theta, \phi)$$

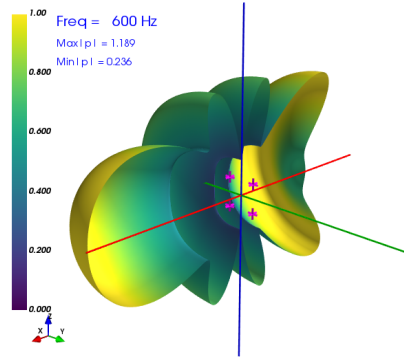
We can apply equations 3.1 and 3.5 to extract the interior source from the mixed source measurements. When we measure in an non-anechoic environment as in figure 1(b), we use equation 3.1 to calculate C_{mn} and D_{mn} . We then substitute C_{mn} into equation 3.5 to reconstruct the sound pressure field with the interior source only. This procedure allows us to recreate the sound pressure field as if the measurements are made in an anechoic environment.

SFS Simulations

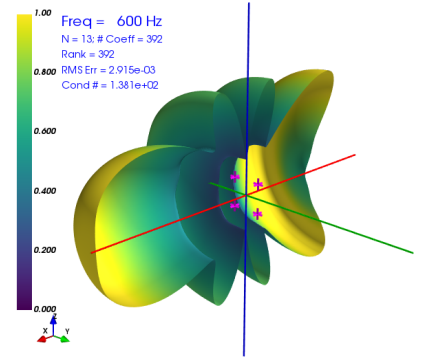
In the figures (2 – 6) showing the simulation results, figures (a) show the reference sound pressure field for the interior sources. This is what we aim to recreate with SFS. Figures (b) show the mixed sources sound pressure field, which simulate the addition of a perfectly reflective wall at $x = -2$ m and are the input data to our reconstructions. Figures (c) show the reconstruction results of the mixed field cases using the method decribed in Part 2, and they should resemble figures (b). Figures (d) to (i) show the results of the free field reconstructions using SFS, and they should resemble figures (a).



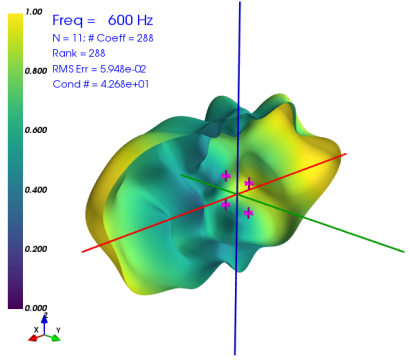
(a) Interior Sources Only (Reference)



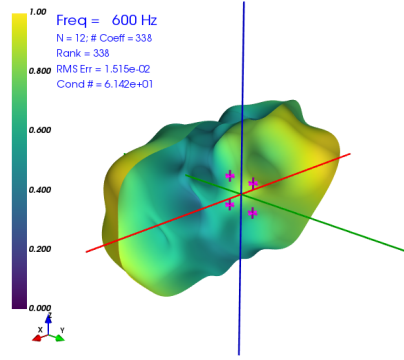
(b) Mixed Sources



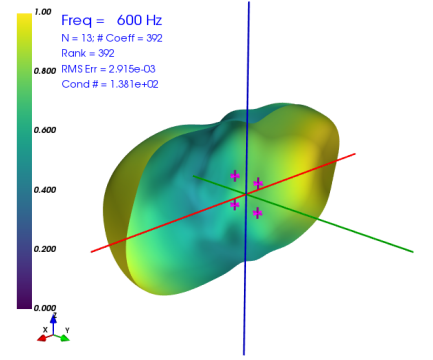
(c) Reconstruction of the Mixed Sources, $N = 13$, no SFS



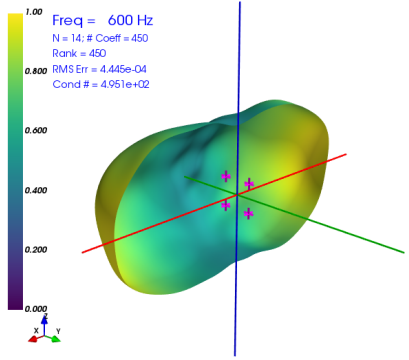
(d) SFS Reconstruction, $N = 11$



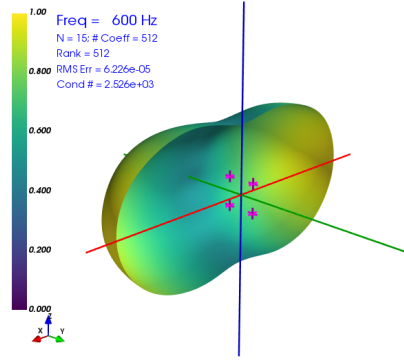
(e) SFS Reconstruction, $N = 12$



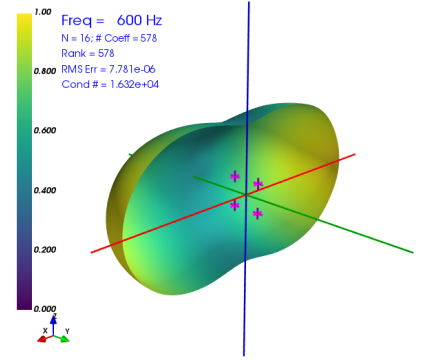
(f) SFS Reconstruction, $N = 13$



(g) SFS Reconstruction, $N = 14$



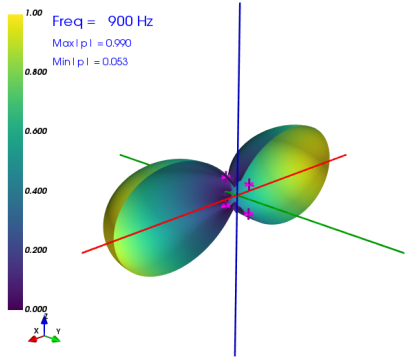
(h) SFS Reconstruction, $N = 15$



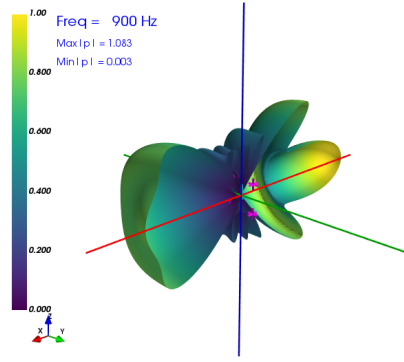
(i) SFS Reconstruction, $N = 16$

Figure 2: Sound Pressure Field Reconstructions at 600 Hz, 1106 Measurement Points

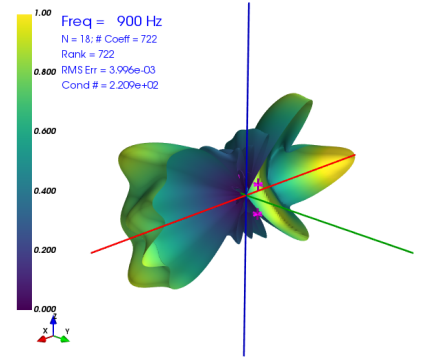
Figure 2 shows the 600 Hz reconstruction results using a 7.5° angular spacing measurement grid and with radial position r varying randomly from 0.95 to 1.05 m. The total number of measurement points is 1106. From the RMS error estimates, we should have achieved satisfactory results by $N = 13$. The SFS reconstruction at $N = 13$ showed a reasonable but far from visually perfect reconstruction. By $N = 15$, the reconstruction is very close.



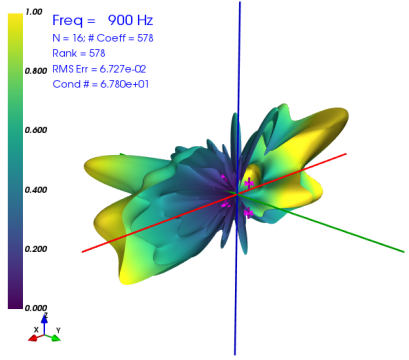
(a) Interior Sources Only (Reference)



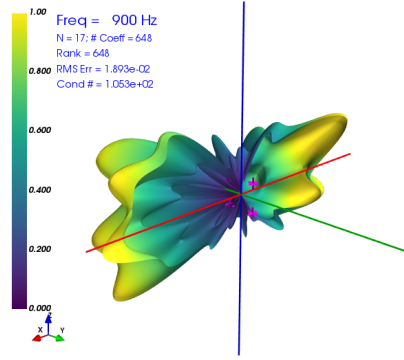
(b) Mixed Sources



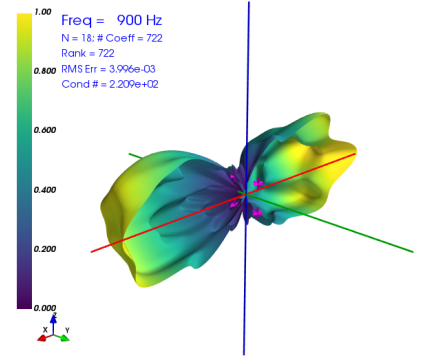
(c) Reconstruction of the Mixed Sources, $N = 18$, no SFS



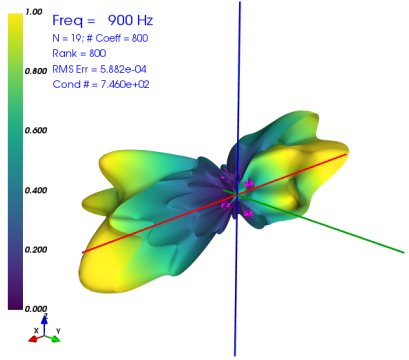
(d) SFS Reconstruction, $N = 16$



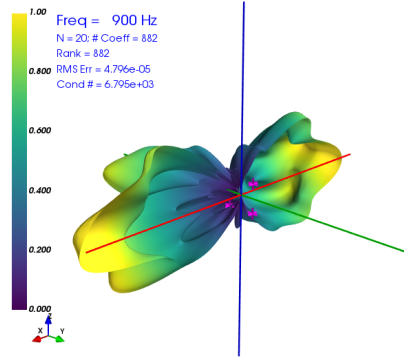
(e) SFS Reconstruction, $N = 17$



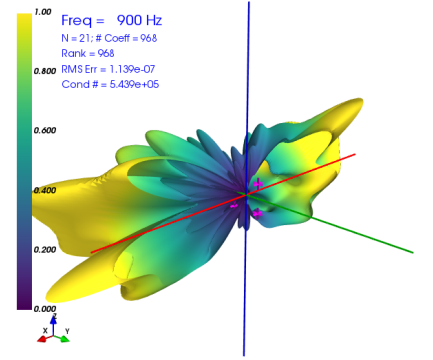
(f) SFS Reconstruction, $N = 18$



(g) SFS Reconstruction, $N = 19$



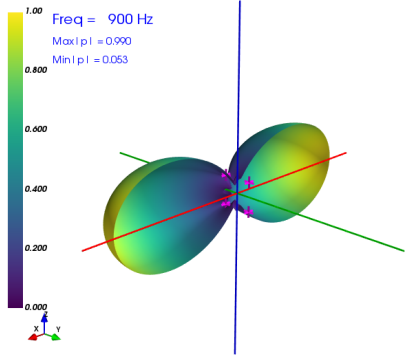
(h) SFS Reconstruction, $N = 20$



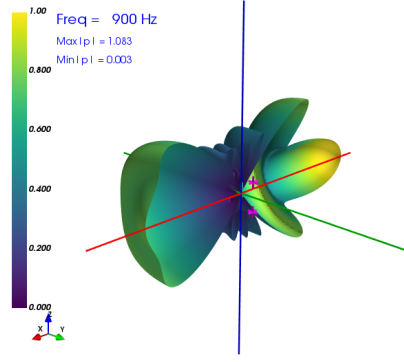
(i) SFS Reconstruction, $N = 21$

Figure 3: Sound Pressure Field Reconstructions at 900 Hz, 1106 Measurement Points

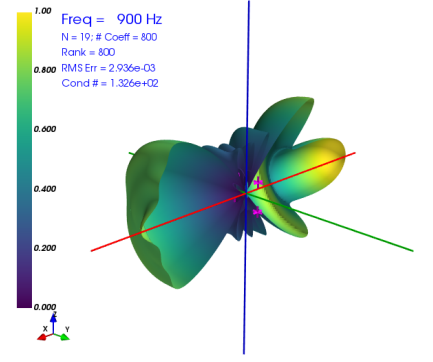
Figure 3 shows the 900 Hz reconstructions. From error estimates, we should have achieved satisfactory results at $N = 18$. Visually, however, there are very noticeable differences between the mixed sources reconstruction (figure 3(c)) and the mixed sources reference (figure 3(b)). The quality of the SFS reconstruction at $N = 18$ is predictably worse (figure 3(f)). Much more notable is that the solutions were not converging. As N increases, the plot shapes diverged instead of stabilizing.



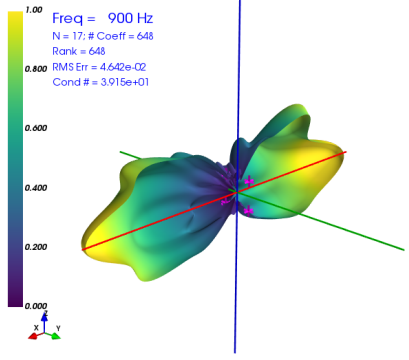
(a) Interior Sources Only (Reference)



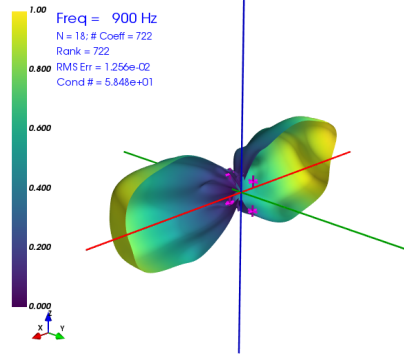
(b) Mixed Sources



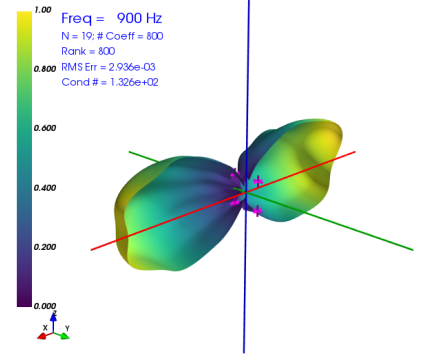
(c) Reconstruction of the Mixed Sources, $N = 19$, no SFS



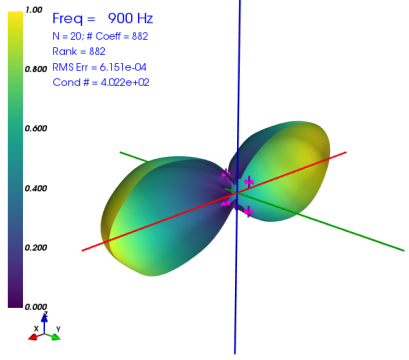
(d) SFS Reconstruction, $N = 17$



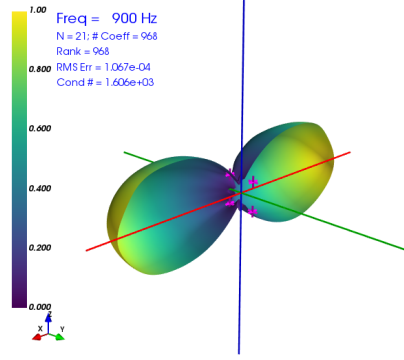
(e) SFS Reconstruction, $N = 18$



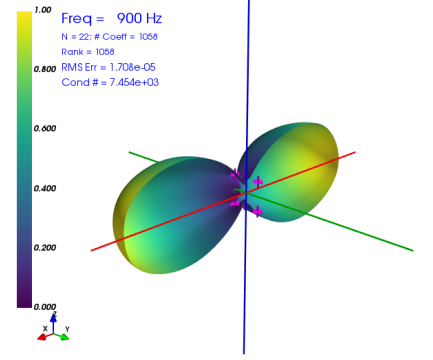
(f) SFS Reconstruction, $N = 19$



(g) SFS Reconstruction, $N = 20$



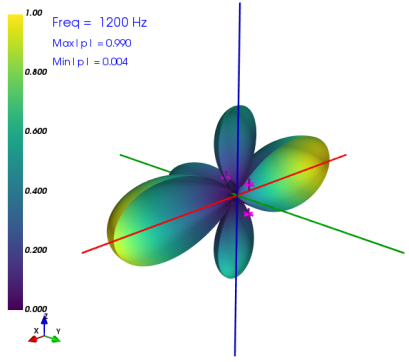
(h) SFS Reconstruction, $N = 21$



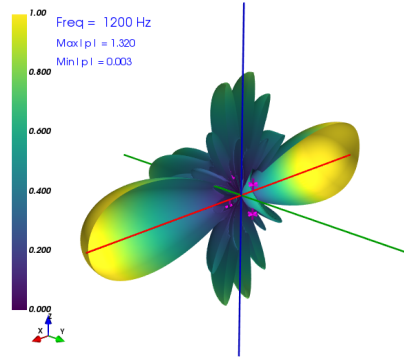
(i) SFS Reconstruction, $N = 22$

Figure 4: Sound Pressure Field Reconstructions at 900 Hz, 2522 Measurement Points

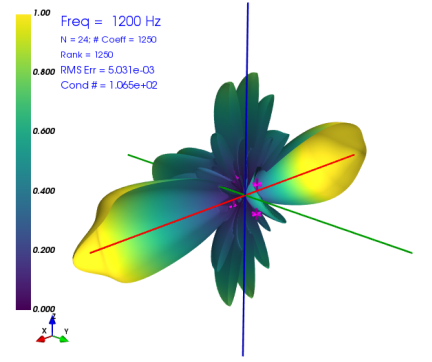
Reducing the measurement grid angular spacing to 5° (number of measurement points increases to 2522) provides significant improvement. The reconstruction solutions converged to the same shape (see figures 4(d) to (i)). At $N = 19$, where the error estimate suggests satisfactory reconstruction, the SFS reconstruction may be adequate if accuracy requirement is low. By $N = 22$, the reconstruction was close to exact.



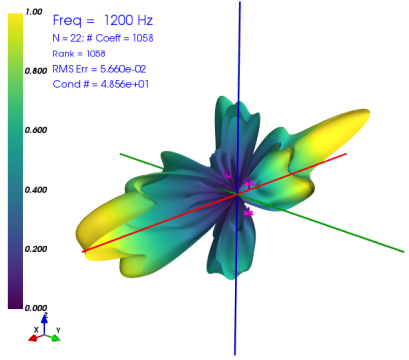
(a) Interior Sources Only (Reference)



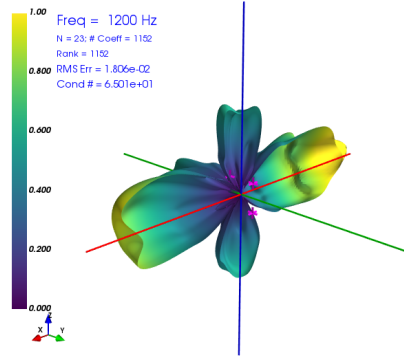
(b) Mixed Sources



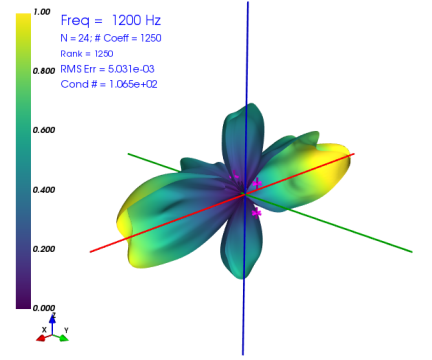
(c) Reconstruction of the Mixed Sources, $N = 24$, no SFS



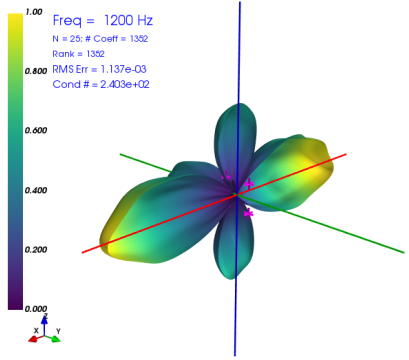
(d) SFS Reconstruction, $N = 22$



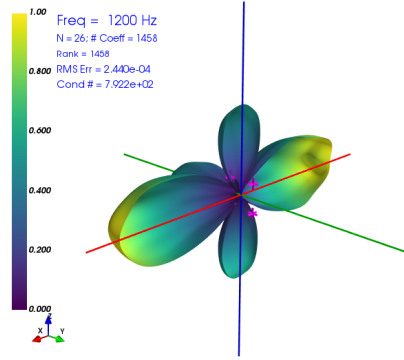
(e) SFS Reconstruction, $N = 23$



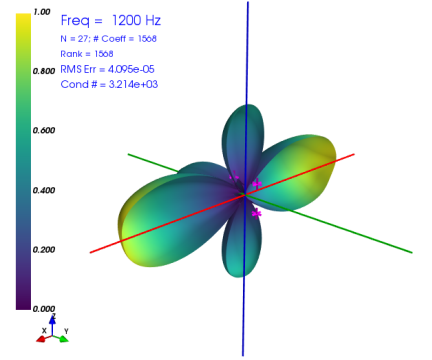
(f) SFS Reconstruction, $N = 24$



(g) SFS Reconstruction, $N = 25$



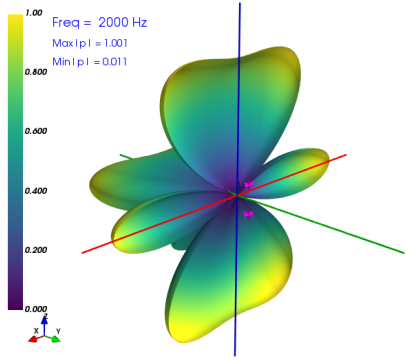
(h) SFS Reconstruction, $N = 26$



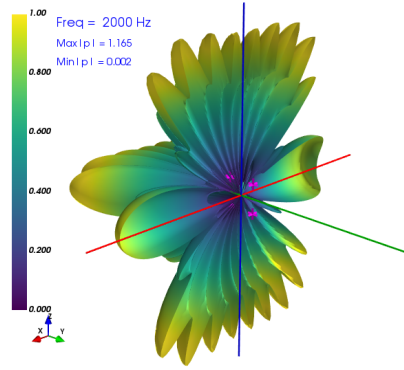
(i) SFS Reconstruction, $N = 27$

Figure 5: Sound Pressure Field Reconstructions at 1200 Hz, 2522 Measurement Points

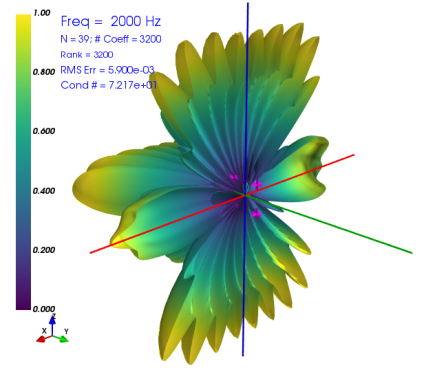
Figure 5 shows the 1200 Hz reconstructions with 2522 measurement points. Error estimates suggest satisfactory reconstruction with $N = 24$. SFS solutions converged. With $N = 24$, the reconstruction resembles the basic shape as in figure 5(a). By $N = 27$, the reconstruction is very close to the reference.



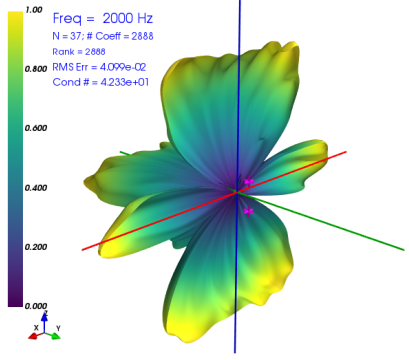
(a) Interior Sources Only (Reference)



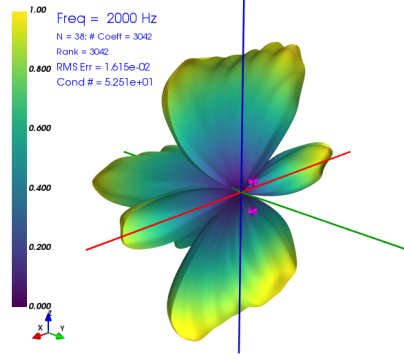
(b) Mixed Sources



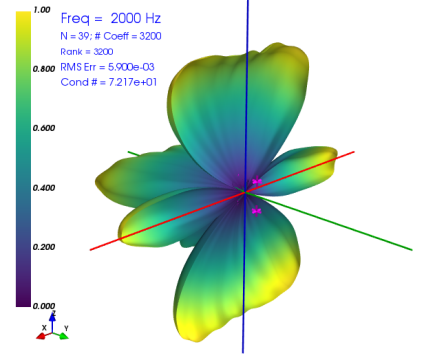
(c) Reconstruction of the Mixed Sources, $N = 39$, no SFS



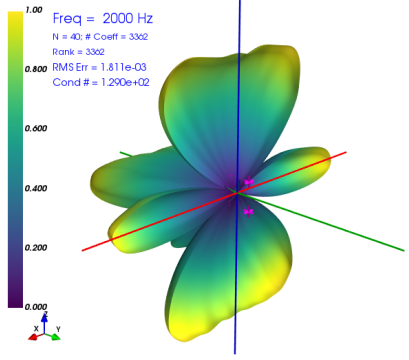
(d) SFS Reconstruction, $N = 37$



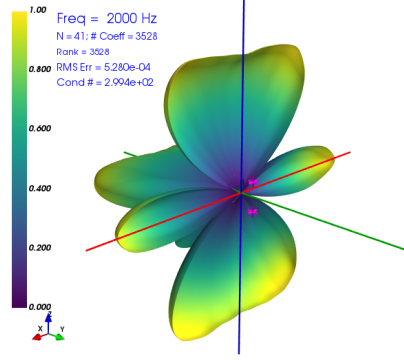
(e) SFS Reconstruction, $N = 38$



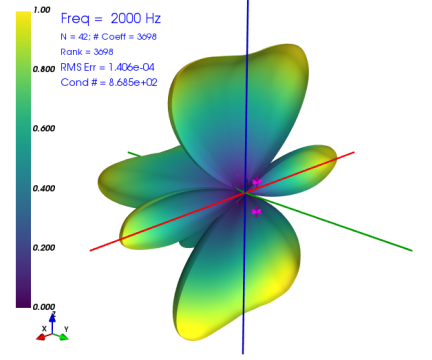
(f) SFS Reconstruction, $N = 39$



(g) SFS Reconstruction, $N = 40$



(h) SFS Reconstruction, $N = 41$



(i) SFS Reconstruction, $N = 42$

Figure 6: Sound Pressure Field Reconstructions at 2000 Hz, 7082 Measurement Points

For 2000 Hz, the solutions failed to converge with measurement grid spacings of 5° and 4° . The results shown are simulated using a 3° grid, requiring 7082 simulated measurement points. Figure 6 shows the reconstructions. Error estimates suggest satisfactory reconstruction with $N = 39$, and the SFS reconstruction at $N = 39$ is a fairly good approximate. By $N = 41$, the reconstruction is very close to the reference.

The trend should be clear by now. Wall reflections complicate the sound pressure field,

especially at higher frequencies. For SFS to work well, it requires a good reconstruction of the mixed sources sound pressure field, and a good reconstruction of a complicated field requires a large number of measurements.

Observations, Discussions and Improvement Ideas

- SFS appears to work quite well for lower frequencies.
- Complicated fields require a large number of measurement points to reconstruct. The pressure fields at higher frequencies tend to be more complicated than at lower frequencies.
- While SFS should help, minimizing room reflections is still beneficial.
- Time windowed impulse measurements may be more practical at the higher frequencies than SFS.
- Error estimates from residuals returned by the least squares solver are not a reliable indicator of the quality of the reconstruction. However, convergence of the solutions, i.e. when the solutions stop changing as N increases, looks to be a good one. This may eliminate the need for a separate test data set, and we can use the entire set of measurements for reconstruction.
- Klippel's recommendation [2, slide 30] of a $1.5\times$ ratio between number of measurement points and number of coefficients ($= 2(N + 1)^2$) seems sound.
- The current measurement grid is not optimized. Optimization may improve accuracy and/or reduce the number of measurement points required.
- Sensitivity to noise and errors in the data has not been not investigated. With the addition of noise and errors, enhancements to the least squares solving method may be required. More elaborate *regularization* techniques may be necessary to reduce their effects.
- It is needless to say that simulations are no substitute for actual testing with real hardware.

Comparison to Other Published SFS Methods

Klippel does not reveal the SFS method they use. The spherical waves expansion equations they show in their publications suggest similar a theoretical basis. However, their measurements are made on two concentric cylindrical surfaces around the loudspeaker under test instead of the spherical surfaces used in this report.

In Zhang et al., they use the following formulations [3, equations 5 and 13]:

$$\text{Mixed fields:} \quad \hat{p}_{mix}(r, \theta, \phi; \omega) = \sum_{n=0}^{\infty} \sum_{m=-n}^n [A_{mn}^{mix} h_n^{(1)}(kr) + B_{mn}^{mix} h_n^{(2)}(kr)] Y_n^m(\theta, \phi)$$

$$\text{SFS Reconstruction:} \quad \hat{p}_{free}(r, \theta, \phi; \omega) = \sum_{n=0}^{\infty} \sum_{m=-n}^n [A_{mn}^{mix} - B_{mn}^{mix}] h_n^{(1)}(kr) Y_n^m(\theta, \phi)$$

A little bit of algebra shows that the method used by Zhang et al. and the method used here are identical. Recall equation 3.4: $C_{mn} = A_{mn} - B_{mn}$, Zhang's SFS reconstruction equation is in fact the same as our equation 3.5.

A SFS method based on double layer spherical measurements was described by Garcia et al. [4]. A different sign convention is used in this paper for the time function (see Part 1), which is why the spherical Hankel function of the second kind $h_n^{(2)}(kr)$ was said to depict the outgoing waves. In this method two measurements are made at each angular coordinate, but each with a different r coordinate. It is believe (but not proven) that, because of the repeated measurements at the same angular coordinate, this method is less efficient in resolving details in the angular directions.

It should also be noted that, in Li et al. [5, section 1.4], they showed that, when using double layer spherical measurements, the *separation distance* (i.e. thickness) of the source free measurement zone should be much less than the wavelength of the sound wave to avoid singularities in the field separation equations. However, this issue was not encountered in the simulations done in this report. This is probably because the radial coordinates r for the measurement points used in the simulations were randomly distributed within the measurement zone and should therefore be without duplication. In the double layer approach, only two values of r are used. If they are selected inappropriately, the system of equations become singular and insolvable. If the requirement of keeping the separation distance much less than the sound wave wavelengths is real, it will render this method impractical for higher frequencies.

References

- [1] S. F. Wu, The Helmholtz Equation Least Squares Method, Springer Science+Business Media New York 2015
- [2] Klippel, Warkwyn, Holographic Measurement of the 3D Sound Field using Near-Field Scanning, 2015, Klippel GmbH, Dresden 01309, Germany
- [3] Peng Zhang, Zheng Kuang, Ming Wu, Jun Yang, A Novel Method for Measuring Acoustic Radiation Fields of Subwoofers Based on Non-Free-Field Aspheric Measurements, 21st International Congress on Sound and Vibration, July, 2014, Beijing/China
- [4] A. Garcia, Y. Braïkia, C. Langrenne, É. Bavu, M. Melon. Source identification in small spaces using field separation method: Application to a car trunk. Proceedings of Acoustics2012, Nantes, France, April 23-27, 2012
- [5] WeiBing Li, MeiZhuan Lian, ChuanXing Bi, Jian Chen and XinZhao Chen, Separation Theory of the Incident and Scattered Sound Fields in Spherical Coordinate, Science in China Series E: Technological Sciences, Science in China Press, Springer-Verlag 2007